Hindawi
Advances in Materials Science and Engineering
Volume 2023, Article ID 5176219, 10 pages
https://doi.org/10.1155/2023/5176219

Research Article

Microstructural Evolution in Nonvacuum Solid-State Diffusion Bonded Joints of AA2219

Manjunath Vatnalmath,[1] **V. Auradi**,[1] **V. Bharath**,[2] **Madeva Nagaral**,[3] **N. Nagaraj**,[4] **and A. Haiter Lenin**[5]

[1]*Department of Mechanical Engineering, Siddaganga Institute of Technology, Visvesvaraya Technological University, Tumakuru 572103, Karnataka, India*
[2]*Department of Mechanical Engineering, RNS Institute of Technology, Visvesvaraya Technological University, Bangalore 560098, Karnataka, India*
[3]*Aircraft Research and Design Centre, HAL, Bangalore 560037, Karnataka, India*
[4]*Department of Mechanical Engineering, APS Polytechnic, Bangalore 560082, Karnataka, India*
[5]*Department of Mechanical Engineering, Wollo University, Kombolcha Institute of Technology, Post Box No. 208, Kombolcha, Ethiopia*

Correspondence should be addressed to A. Haiter Lenin; haiterlenina@gmail.com

Received 12 August 2022; Revised 16 September 2022; Accepted 16 January 2023; Published 31 January 2023

Academic Editor: Adam M. Khan

Solid-state diffusion bonding of AA2219 alloy is carried out under the nonvacuum condition to form AA2219/AA2219 joints. In the currently adopted method, AA2219 alloys are joined under the bonding temperature of 450–500°C, bonding pressure of 10 MPa, and bonding time of 30 min. Chemical cleaning is adopted to protect the joining surfaces from reoxidation before the diffusion bonding process. Microstructure evolution at the bonded joints is characterized using optical microscopy, scanning electron microscopy (SEM), and energy dispersive spectroscopy (EDS). The hardness at the bonded joints increased with the increase in the bonding temperature. The parent metal structure is achieved at 500°C bonding temperature with an increase in hardness of 112.14 Hv at the bond interface. There is no evidence of intermetallic found at the interface, as confirmed by X-ray diffraction (XRD).

1. Introduction

Isogrid structures have gained much attention in the aerospace industry due to their lightweight properties and high strength-to-weight ratios, specifically for launching vehicle structures. AA2219 is one such copper aluminium alloy that is primarily used for producing the isogrid structures due to its high weldability, stress corrosion cracking resistance, and excellent mechanical properties at cryogenic temperatures [1–3]. AA 2219 has already been used successfully in several launch vehicle systems, such as Saturn V and the Apollo Space Shuttle, and it was also chosen for Ariane V to replace AFNOR 7020 [4]. Joining similar and dissimilar metal alloys has become increasingly challenging to combine the various material properties to achieve lightweight properties and high product performance in industries like aerospace and automotive [5, 6]. While joining the different metal alloys, the differences in physical and thermal properties would become the main hurdles [7–9]. The major difficulty in joining aluminium and its alloys by conventional and even advanced welding techniques is the tenacious oxide film that exists on the faying surfaces, acting as a strong barrier for atomic interdiffusion [10, 11]. Though the welding properties of the AA2219 are superior to those of other aluminium alloys, the welded joints exhibit poor strength even when using advanced welding techniques such as gas metal arc welding (GMAW), gas tungsten arc welding (GTAW), and plasma

arc welding (PAW). The loss in joint strength is mainly due to the melting and quick solidification of the metal involved in these welding processes [12]. The welding of components with complex internal structures is challenging with advanced solid-state welding methods like friction stir welding (FSW) [13].

To overcome such difficulties, the diffusion bonding techniques are used more prominently, as they do not induce macroscopic material deformation, preserving the parent metal strength and reducing the oxide formation at the joints. [14–17]. Solid-phase diffusion bonding is highly preferred for numerous industrial products where the welding is to be formed without any liquid phases [18, 19]. Diffusion bonding is usually carried out at the temperature range of 50–80% of the melting temperature of the metal, and the quality of the bonding joints mainly depends on the process variables such as temperature, pressure, and time [20, 21]. However, the adherent and chemically stable oxide films on the faying surface of the aluminium and its alloys must be removed before the diffusion bonding process to curb the formation of metallurgical differences at the bonded joints [22, 23]. The prior cleaning of the faying surface of aluminium with alkaline and acidic solutions is one such technique to minimize the formation of oxides during diffusion bonding [24–26].

Generally, the diffusion bonding process is carried out in a vacuum [27, 28] or an inert [29, 30] chamber to eliminate the formation of oxides at the interface. However, Pilling and Ridley [31] emphasized the vacuum-free solid-state diffusion bonding of AA7475 conducted in a furnace attached to an Instron universal testing machine (UTM) by employing a chemical pickling of the faying surfaces of aluminium alloy before the diffusion bonding process to inhibit the oxide formation at the interface. Jia et al. [32] investigated the diffusion bonding of Al 6061 by cladding Zn material, and Liu et al. [33] employed the electrodeposition of nano-Cu to join Al-Mg-Li alloys, mainly to inhibit the oxidation at the interface.

This research study focused on conducting a nonvacuum solid-state diffusion bonding of AA2219. The aluminium surfaces would oxidise rapidly, and this certainly prevents the better surface contact required for the perfect diffusion bonding. Hence, a chemical cleaning of the faying surface is employed to reduce the effect of oxidation at the interface. The bonding temperature is chosen in the range of 450–500°C with constant bonding pressure and time. Microstructural investigations are carried out to evidence the oxide formation on the bonded and unbonded interfaces.

2. Experimental Procedure

AA2219-T6 plates are sectioned to the dimensions of 50 mm × 40 mm × 8 mm with the help of wire cut electric discharge machining (EDM). The chemical composition of AA2219 is represented in Table 1.

Table 1: Chemical composition of AA2219 (wt. %).

Si	Fe	Cu	Mn	Mg	Zn	Ti	V	Zr	Al
0.20	0.30	5.8	0.20	0.02	0.10	0.02	0.05	0.1	Bal

The faying surfaces of the base metal plates are initially prepared on grit SiC papers up to a 1000 grit finish and then degreased using acetone before the chemical cleaning process. The prepared base metals are immersed in a novel chemical solution containing sodium salts and sodium hydroxide at 120°C for 1 minute, then immersed in 40% HNO_3 for 1 minute, water flushed, cleaned in an acetone bath, and dried in hot air. Once the chemical cleaning is finished immediately, the diffusion bonding is carried out by stacking the AA2219 plates in customized diffusion bonding equipment. The schematic illustration of the diffusion bonding setup is shown in Figure 1.

The combinations of temperature, pressure, and time can be used to get a good metallurgical bond of the various metals, and these combinations of parameters would be independent of the structure to be fabricated [34]. The nonvacuum diffusion bonding is performed at the bonding temperatures of 450, 475, and 500°C by maintaining pressure and time constants. The specimens are soaked to the bonding temperature at a heating rate of 6°C/min. A bonding pressure of 10 MPa is applied for a holding duration of 30 min. Although the diffusion bonding is tested for 1, 2, 5, and 7 MPa for the mentioned bonding temperatures, the bonding did not occur mainly due to the insufficient pressure to catalyze the interdiffusion for the shorter bonding duration of 30 min. Figure 2 shows the schematic representation of the bonding parameters.

The bonded specimens are furnace cooled without releasing the pressure to avoid thermal shocks. Figures 3(a) and 3(b) show a bonded specimen immediately after removing from the furnace and the polished surface of its bonded section.

The furnace-cooled specimens are sectioned perpendicularly to the bonded line using wire cut EDM. The resulting surfaces are polished using the diamond suspension and then etched with the help of Kellers reagent as per E 407-07 (microetching metals and alloys) [35] before the metallographic analysis. The microstructures of the bonded joints are examined using an optical microscope and the scanning electron microscope (SEM), and variations in composition across the joint sections are examined through energy dispersive spectroscopy (EDS). The hardness of the joints, across the section and base metals, is measured as per ASTM standard E-384 [36] using a Vickers microhardness tester with an indentation load of 200 gm.

3. Results and Discussion

3.1. Microstructural Evolution. The microstructures of the bonded specimens are pre-examined carefully at the joints, interfaces, and base of the metals by using a light optical microscope. Figures 4(a) and 4(b) show the optical micrographs of bonded specimens produced at 450°C. The micrograph in Figure 4(b) reveals that the diffusion and some migrated diffusion lines are visible at the interface of the bonded metals. Interfacial voids are exhibited along the diffusion line, which depicts the incomplete bonding at the interface.

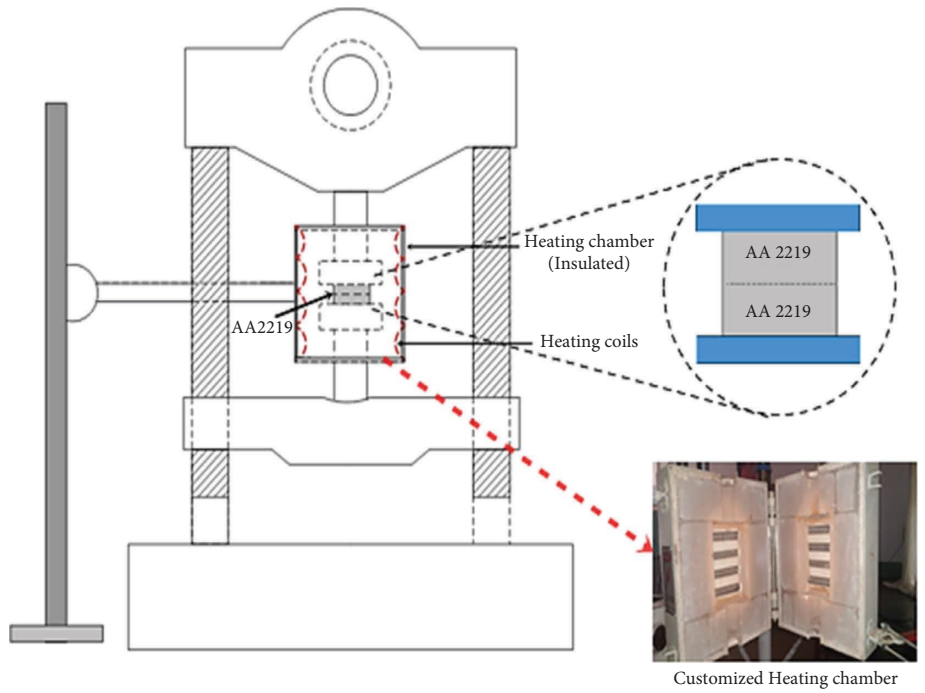

Figure 1: Schematic representation of the customized diffusion bonding equipment.

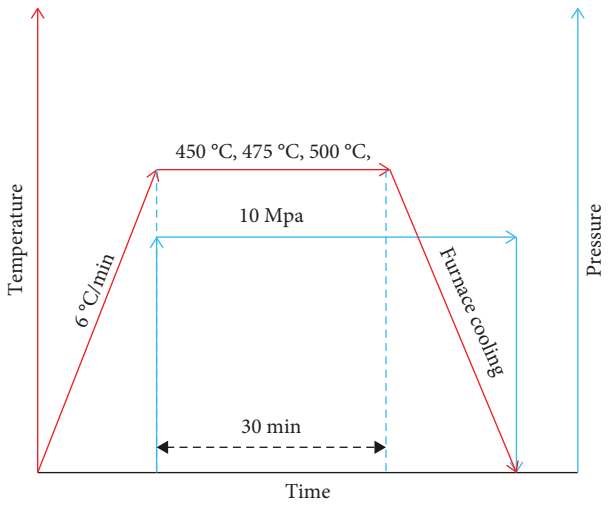

Figure 2: Schematic diagram of the diffusion bonding parameters.

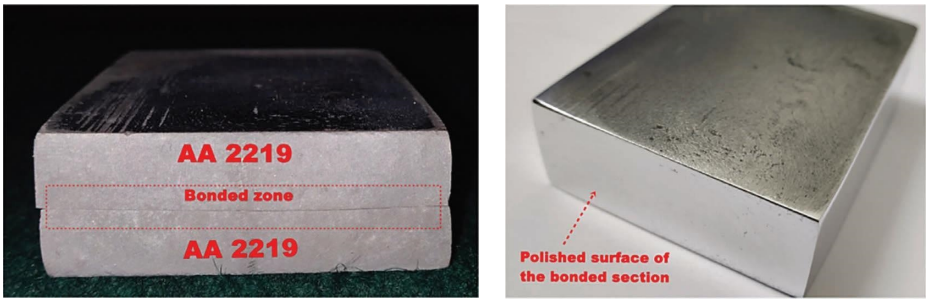

(a) (b)

Figure 3: (a) Diffusion bonded AA 2219 alloy and (b) polished surface of the bonded section.

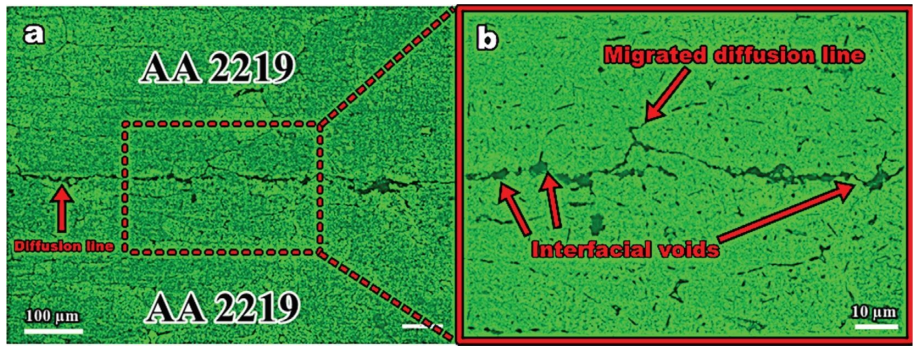

Figure 4: (a) Optical micrographs of the section bonded at 450°C and (b) enlarged view of the rectangular drawn in (a).

The interfacial grain growth is visible with a very thin diffusion line on the sections bonded at 475°C which are shown in Figures 5(a) and 5(b). This certainly indicates that the interdiffusion is catalyzed by the increase in temperature. However, the perfectly bonded specimens do not exhibit any metallurgical evidence of a diffusion line or interface by forming a monolithic joint [25]. Figure 6 shows the micrographs of such undistinguishable microstructures on the sections, obtained at the temperature of 500°C. From the optical micrographs in Figure 6, it is evident that local expulsion of interfacial boundaries steers the reformation of grains across the interface then finally forming a homogeneous microstructure without showing evidence of any bond line or interface.

Further analysis is carried out using SEM to analyze the bonded joints and interfaces more acutely. The voids and the bonded areas on the interface are mainly investigated to know the mechanisms of diffusion bonding and oxide behaviour with respect to temperature change. The SEM micrographs of the bonded section at 450°C are shown in Figures 7(a) and 7(b), which show that microvoids are exhibited continuously along with the interface of the faying surfaces. A few bonded areas are visible on the interface which signifies the lack of a complete bond. When the bonding temperature further increased to 475°C, the voids are crushed to form a hardly visible bond line, and the grain growth occurred across the interface, which is represented in Figures 8(a) and 8(b). The sections bonded at 475°C also exhibit minute voids, infrequently at some parts of the interface and thin precipitations persist on the bond line as shown in the detailed view in Figure 8(b), which are certainly the main causing factors for the incomplete grain growth across the interface [37]. At a bonding temperature of 500°C, however, a complete grain development across the interface by producing a single homogeneous structure is achieved, which is shown in Figure 9. There is no evidence of voids, and precipitates form on the sections bonded at 500°C, which ensures the formation of triple-point junctions at the intervals of the grains near the interface [38].

In this study, the complete diffusion bonding process is carried out in the air, so there is always a risk of oxide formation on the interfaces. The sections bonded incompletely by forming voids and cracks on the interfaces, which undeniably show the oxide formations. In the course of the diffusion bonding process in air, the faying surfaces always reoxidize and prevent complete atomic contacts at the interface. At higher temperatures, total atomic contact can be achieved at the interface by fracturing the oxide layers, and the voids are coalesced by aluminium diffusion, resulting in a complete bond [31]. This study, without reserving emphasized the oxide behaviour across the diffusion interface and voids. Figures 10(a), 10(b), 11(a), 11(b), 12(a), and 12(b) show EDS and spectral analysis of bonded sections obtained at 450°C, 475°C, and 500°C, respectively. From Figures 10(b) and 11(b), it is evident that bonded areas on the interfaces obtained at 450 and 475°C indicate a slight oxide mass in the range of 2–3.7% whereas a similar study with transient liquid phase (TLP) diffusion bonding using a nano-Cu interlayer has shown an oxide mass in the 5–8% range on the interface [33].

Figures 13(a) and 13(b) show the EDS and spectral analysis of larger voids present on the interface of the bonded section at 450°C. The larger voids present on the interface of bonded sections at 450°C exhibit higher oxides as they are always critically exposed to air. Figure 13(b) reveals the existence of an excess oxide mass of 14.3%. However, the presence of higher oxide on the interface would also be due to the formation of fine particles of aluminium oxide developed from the shearing of oxide layers [39].

Despite this, the complete bonding obtained at 500°C exhibits the undistinguishable microstructure, and that does not much signify the presence of oxides, as the complete atomic diffusion occurred between the two faying surfaces at this temperature, which is quantified in Figure 12(b). The XRD patterns of the specimen bonded at 500°C are measured, as shown in Figure 14, to further confirm the intermetallic phases in the joint area. The diffraction peak cannot be observed due to the low composition of the second phase, and all the peaks in the pattern are confirmed to Aluminium. As a result, there are relatively few second phases in the joint that cannot be detected by XRD.

3.2. Mechanical Characterization. The hardness behaviour of the joints obtained at 450°C, 475°C, and 500°C is assessed by the microhardness test by focusing on the vicinity of the bond interfaces, and the corresponding results are shown in Figure 15. The hardness on the bonded line of the section obtained at 450°C is 68.12 Hv, while the higher values of hardness are observed on the points away from the bond

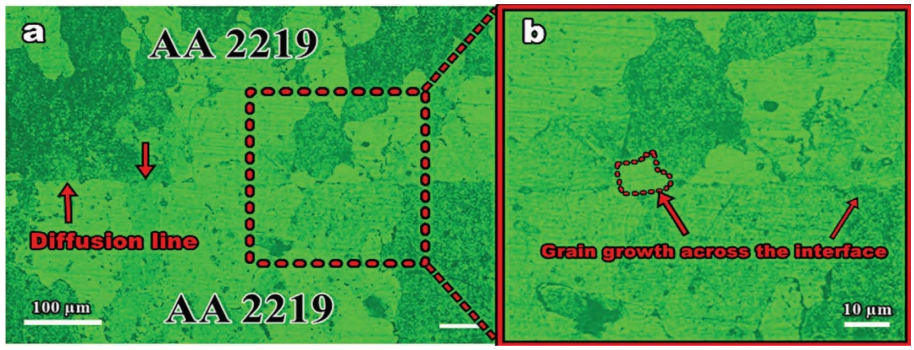

Figure 5: (a) Optical micrographs of the section bonded at 475°C and (b) enlarged view of the rectangular drawn in (a).

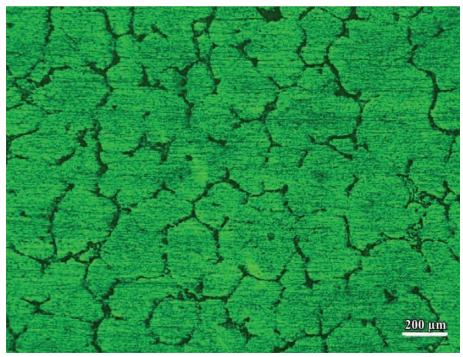

Figure 6: Optical micrographs of the section bonded at 500°C.

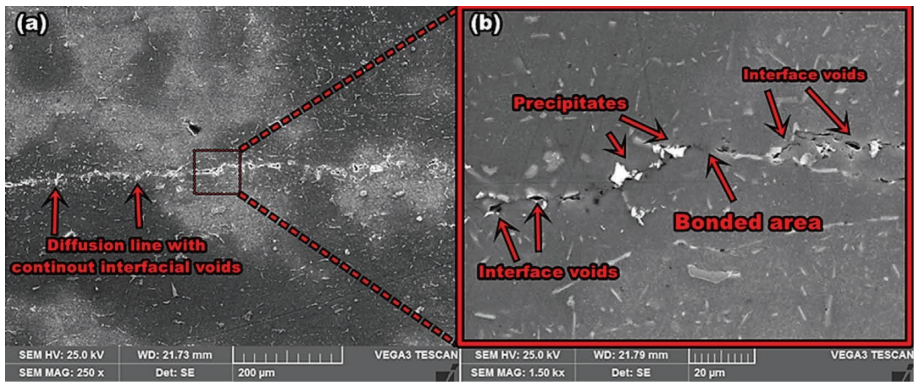

Figure 7: (a) SEM micrographs of the section bonded at 450°C and (b) detailed view of the rectangular drawn in (a).

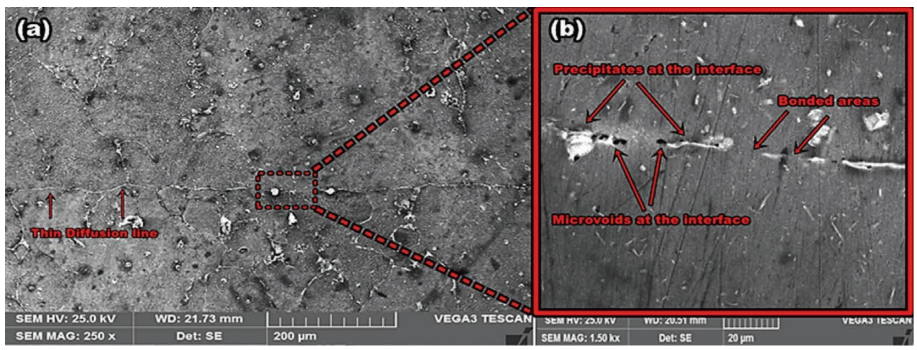

Figure 8: (a) SEM micrographs of the section bonded at 475°C and (b) detailed view of the rectangular drawn in (a).

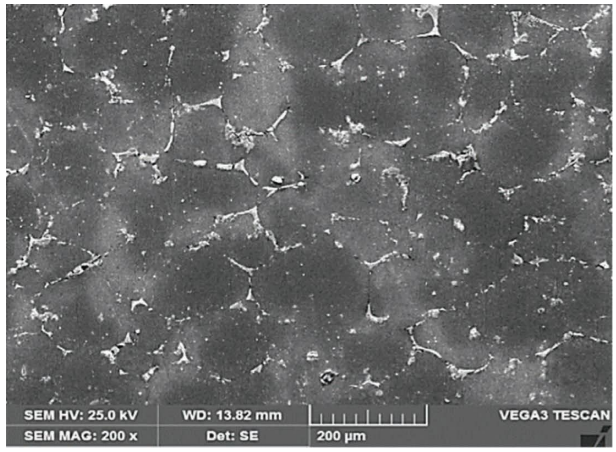

Figure 9: SEM micrograph of the section bonded at 500°C.

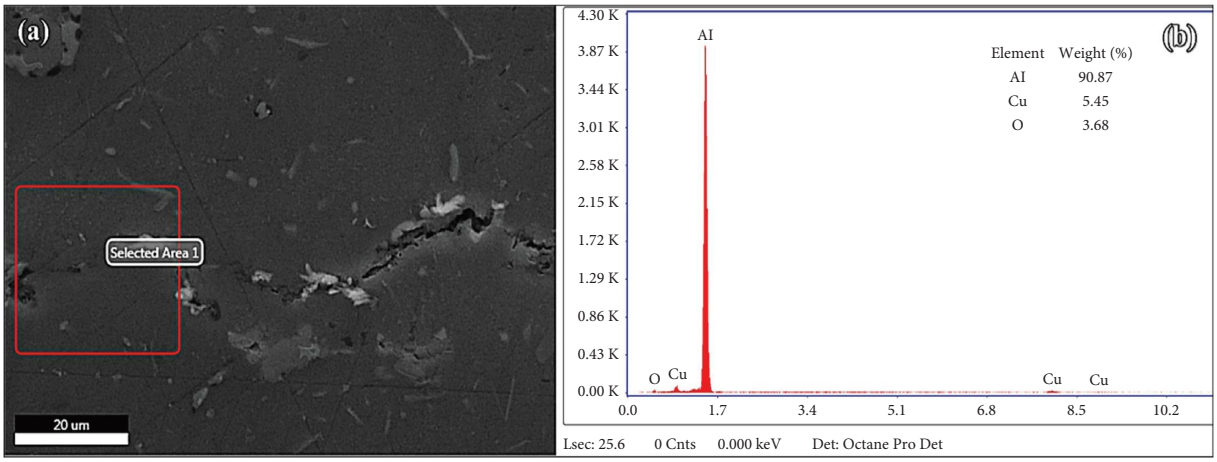

Figure 10: (a) EDS and (b) spectral analyses for the bonded area on the interface at 450°C.

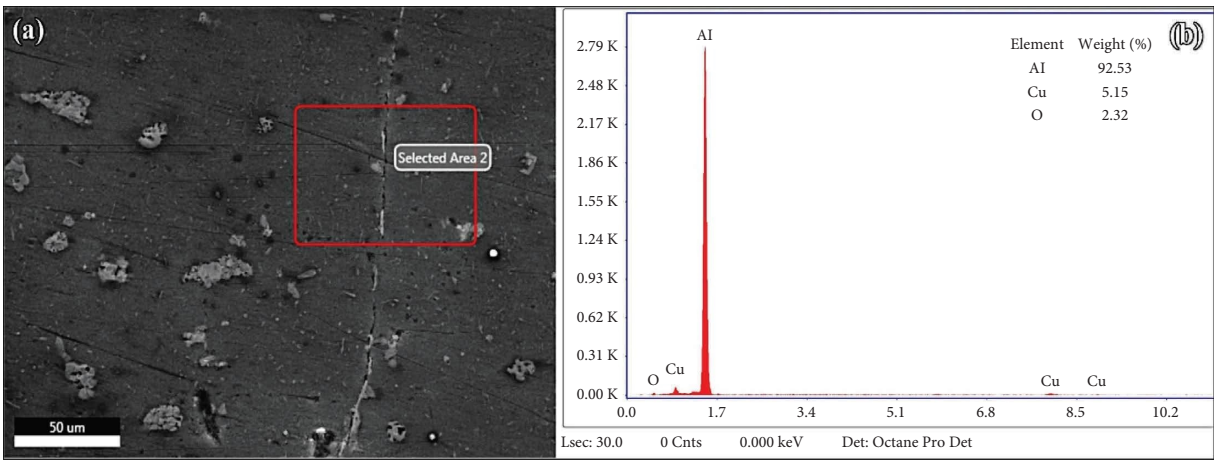

Figure 11: (a) EDS and (b) spectral analyses for the unbonded area on the interface at 475°C.

line. The drastic reduction in hardness is mainly because of the absence of grain growth across the interface, continuous interfacial voids, and oxide formed in the joint regions. The bond interface made at 475°C exhibited a hardness of 102.82 Hv, and this value is relatively higher than the base material. A slight increase in hardness due to the cause of thin precipitates formed on the interface of the faying surfaces. Table 2 shows the influence of bonding temperature

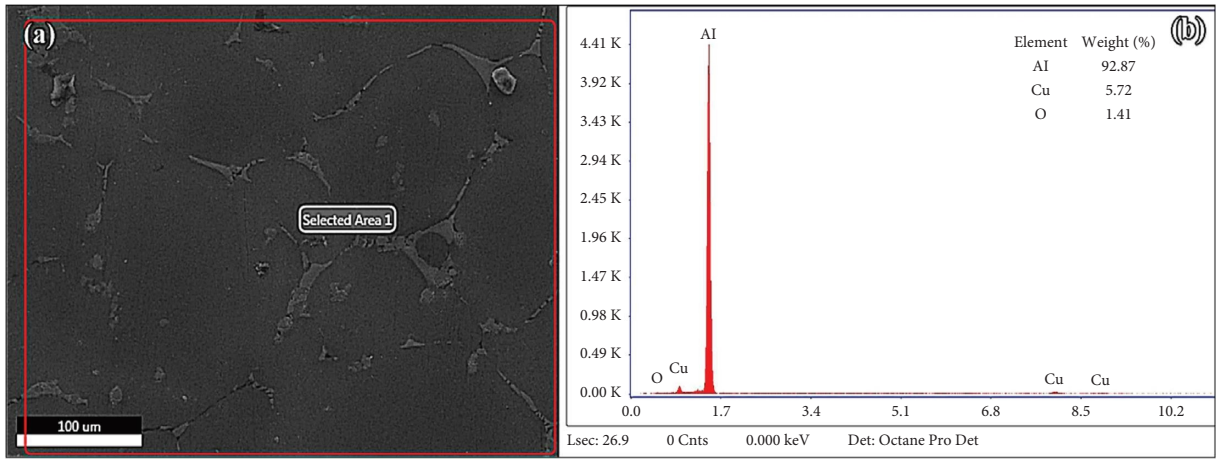

Figure 12: (a) EDS and (b) spectral analyses for interface area of bonded section at 500°C.

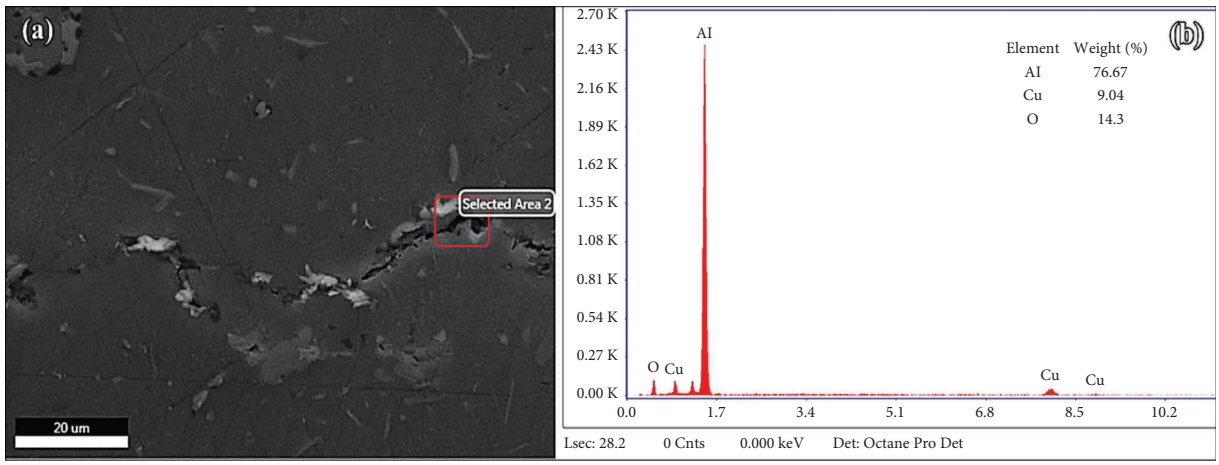

Figure 13: (a) EDS and (b) spectral analyses for the bonded section at 450°C.

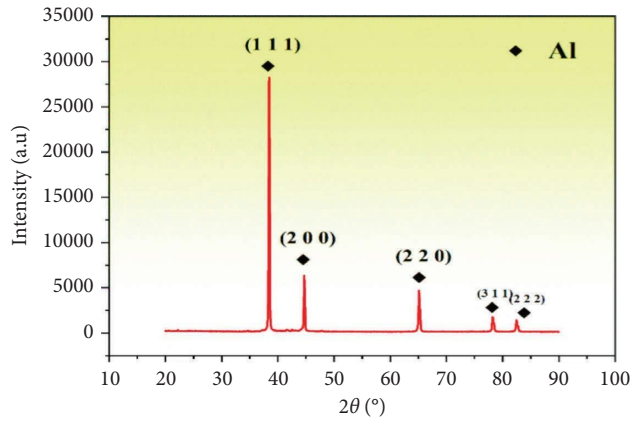

Figure 14: XRD analysis of specimen bonded at 500°C.

on the hardness of the bonded sections. The hardness values at the interfaces are increased with the rise in the bonding temperature.

However, as the bonded sections obtained at 500°C do not reveal any diffusion line or interface, an average of 15 readings was taken at different intermittent points on and

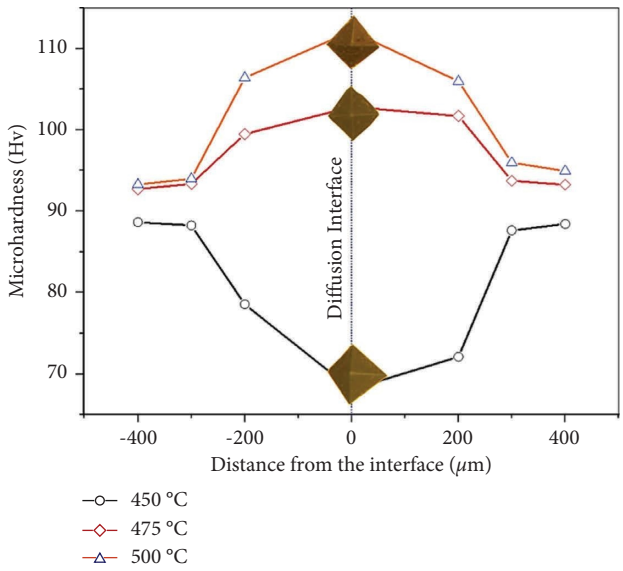

Figure 15: Microhardness behaviour across the bonded interface as a function of bonding temperature.

Table 2: Influence of bonding temperature on the hardness of bonded sections.

Bonding conditions			Hardness on		
Temperature (°C)	Pressure (MPa)	Time (min)	Base metal (left)	Interface (center)	Base metal (right)
450	10	30	88.63	68.12	88.42
475	10	30	92.71	102.82	93.25
500	10	30	93.28	112.14	94.94

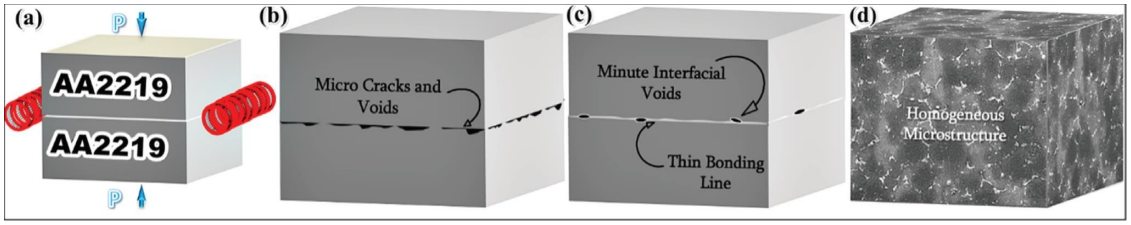

Figure 16: Bonding formations of the AA2219 joints: (a) Specimens before diffusion bonding, (b) formation of cracks and voids along the interface at 450°C, (c) formation of thin bonding line on the interface at 475°C, and (d) formation of the homogeneous microstructure without bonding line at 500°C.

from the center of the bonded section. The points at the center show (Figure 15) a maximum hardness of 112.14 Hv, whereas hardness has been reduced while testing on the points away from the center. The changes in hardness values at the interface are mainly due to the sound joint formed by the coarsening of precipitates with the increase in temperature at the bonded zone [37] whereas a similar diffusion bonding study conducted in an inert atmosphere reported approximately the same hardness value at the interface and base materials [25].

4. Summary

Figure 16 shows the schematic representation of the bonding formation of AA2219 joints. Initially, when the specimens are stacked on top of one another, an incomplete contact is formed due to the presence of asperities on the metal surfaces. When the bonding temperature increased to 450°C with the application of 10 MPa pressure for the bonding duration of 30 minutes, the asperities are deformed and a large number of microcracks and voids are formed along the interface of metals (Figure 16(b)). It is mainly due to the insufficient temperature offered for the deformation of the boundaries and the interdiffusion of atoms. A thin bonding line with minute voids and precipitates is observed due to the microplastic deformation of the metal boundaries at the bonding temperature of 475°C (Figure 16(c)). However, when the temperature increased to 500°C, recrystallization occurred at the metal boundaries, and upon solidification, no metallurgical evidence of microvoids and bonding lines are seen. The joints produced at this bonding temperature show a good hardness value compared to the joints obtained at 450°C and 475°C.

5. Conclusion

AA2219/AA2219 bonded joints are successfully formed using a nonvacuum solid-state diffusion bonding process performed in atmospheric air without incorporating cladding or electrodepositing other metals. The efficiency of the nonvacuum diffusion bonding of aluminium alloys by employing chemical redox agents is found to be feasible. The influence of bonding temperature on the microstructure and hardness of the joint interfaces are studied by keeping the pressure and time constant.

(i) Grain boundary expulsion and grain growth across the interface are observed on all the bonded sections. However, this condition is found only in some random areas of the bonded sections between 450 and 475°C.

(ii) Relatively a quality bond with homogeneous microstructure and without showcasing any metallographic evidence of bond line has been achieved under the bonding temperature of 500°C.

(iii) Incomplete bonded sections exhibit interfacial voids with a higher mass percentage of oxide compared to the perfectly bonded sections.

(iv) As the bonding temperature increased, the hardness at the bond interfaces increased due to the elimination of voids and oxides. The bonded interface obtained at 500°C yielded a maximum microhardness of 112.14 Hv.

Data Availability

No data were used to support this study.

Conflicts of Interest

The authors declare that they have no conflicts of interest.

Acknowledgments

The authors would like to thank the All India Council for Technical Education (AICTE), New Delhi, for financial assistance in carrying out the research work (Grant no. 8-114/FDC/RPS(POLICY-1)/2019-20). This work received financial support from AICTE, New Delhi, under the Research Promotion Scheme (File No. 8-114/FDC/RPS (Policy-1)/2019-20)) for carrying out the current research work and is highly acknowledged.

References

[1] H. Yang, L. Liu, H. Chen, L. Wang, and Q. Tong, "Investigation on creep age forming of AA2219 stiffened structures," *MATEC Web of Conferences*, vol. 21, p. 4010, 2015.

[2] T. Ramkumar, A. Haiter Lenin, M. Selva kumar, M. Mohanraj, S. C. Ezhil Singh, and M. Muruganandam, "Influence of rotation speeds on microstructure and mechanical properties of welded joints of friction stir welded AA2014-T6/AA6061- T6 alloys," *Proceedings of the Institution of Mechanical Engineers - Part E: Journal of Process Mechanical Engineering*, vol. 9, Article ID 95440892210776, 2022.

[3] S. K. Manwatkar, M. Sunil, A. Prabhu, S. V. S. Narayana Murty, R. Joseph, and P. Ramesh Narayanan, "Effect of grain size on the mechanical properties of aluminum alloy AA2219 parent and weldments at ambient and cryogenic temperature," *Transactions of the Indian Institute of Metals*, vol. 72, no. 6, pp. 1515–1519, 2019.

[4] P. Srinivasa Rao, K. G. Sivadasan, and P. K. Balasubramanian, "Structure-property correlation on AA 2219 aluminium alloy weldments," *Bulletin of Materials Science*, vol. 19, no. 3, pp. 549–557, 1996.

[5] K. Martinsen, S. J. Hu, and B. E. Carlson, "Joining of dissimilar materials," *Cirp Annals*, vol. 64, no. 2, pp. 679–699, 2015.

[6] H. Wargnier, F. X. Kromm, M. Danis, and Y. Brechet, "Proposal for a multi-material design procedure," *Materials and Design (1980-2015)*, vol. 56, pp. 44–49, 2014.

[7] H. Shi, S. Qiao, R. Qiu, X. Zhang, and H. Yu, "Effect of welding time on the joining phenomena of diffusion welded joint between aluminum alloy and stainless steel," *Materials and Manufacturing Processes*, vol. 27, no. 12, pp. 1366–1369, 2012.

[8] A. Anbarzadeh, H. Sabet, and M. Abbasi, "Effects of successive-stage transient liquid phase (S-TLP) on microstructure and mechanical properties of Al2024 to Ti-6Al-4V joint," *Materials Letters*, vol. 178, pp. 280–283, 2016.

[9] A. N. Alhazaa and T. I. Khan, "Diffusion bonding of Al7075 to Ti–6Al–4V using Cu coatings and Sn–3.6 Ag–1Cu interlayers," *Journal of Alloys and Compounds*, vol. 494, no. 1-2, pp. 351–358, 2010.

[10] X. G. Wang, X. G. Li, and C. G. Wang, "Transient liquid phase bonding of aluminium alloy using two-step heating process," *Science and Technology of Welding and Joining*, vol. 17, no. 5, pp. 414–418, 2012.

[11] K. Ikeuchi, F. Matsuda, and K. Kotani, "Behaviour of oxide at diffusion-bonded interfaces in Al-Mg-Si series 6063 alloy: study of diffusion-bonding mechanism of aluminium alloys by transmission electron microscopy (1st Report)," *Welding International*, vol. 10, no. 9, pp. 697–704, 1996.

[12] S. Malarvizhi and V. Balasubramanian, "Effect of welding processes on AA2219 aluminium alloy joint properties," *Transactions of Nonferrous Metals Society of China*, vol. 21, no. 5, pp. 962–973, 2011.

[13] P. Y. Ma, X. Chen, X. Han, Z. Q. Luo, and H. Peng, "Effect of bonding temperature and heat treatment on microstructure and mechanical property of Mg– 6Gd– 3Y alloy vacuum diffusion bonded joints," *Transactions of Nonferrous Metals Society of China*, vol. 32, no. 7, pp. 2205–2215, 2022.

[14] M. Samavatian, A. Khodabandeh, A. Halvaee, and A. A. Amadeh, "Transient liquid phase bonding of Al 2024 to Ti–6Al–4V alloy using Cu–Zn interlayer," *Transactions of Nonferrous Metals Society of China*, vol. 25, no. 3, pp. 770–775, 2015.

[15] Y. Wei, F. Sun, S. Tan, and S. Liang, "Study on microstructure and performance of transient liquid phase bonding of Cu/Al with Al-based interlayers," *Vacuum*, vol. 154, pp. 18–24, 2018.

[16] B. A. Kumar, M. M. Krishnan, A. F. Sahayaraj et al., "Characterization of the aluminium matrix composite reinforced with silicon nitride (AA6061/Si3N4) synthesized by the stir casting route," *Advances in Materials Science and Engineering*, vol. 2022, Article ID 8761865, 8 pages, 2022.

[17] A. Arun Negemiya, A. N. Shankar, B. Guruprasad et al., "Investigation on processing maps of diffusion bonding process parameters for Ti-6Al-4 V/AISI304 dissimilar joints,"

Advances in Materials Science and Engineering, vol. 2021, Article ID 5601970, 9 pages, 2021.

[18] R. Rusnaldy, "Diffusion bonding: an advanced of material process," *Rotasi*, vol. 3, no. 1, pp. 23–27, 2001.

[19] H. S. Lee, "Application of Solid State Welding and Superplastic Forming to Aerospace Vehicles," Society of Automotive Engineers International, Warrendale, PE, USA, SAE Technical Paper, 2017.

[20] W. Melik, Z. Boumerzoug, and F. Delaunois, "Solide state diffusion bonding of Al6061-SiC nanocomposites," *International Journal of Automotive and Mechanical Engineering*, vol. 18, no. 4, pp. 9305–9311, 2021.

[21] Y. Peng, J. Li, Z. Li et al., "Interfacial voids and microstructure evolution, bonding behavior and deformation mechanism of TC4 diffusion bonded joints," *Journal of Manufacturing Processes*, vol. 81, no. 2022, pp. 837–851, 2022.

[22] D. Palanisamy, A. Sagai Francis Britto, J. S. Binoj, and N. Manikandan, "Statistical optimization of parameters for enhanced properties of diffusion bonded AA6061 and AA 7075 aluminium alloys," *Materials Today Proceedings*, vol. 39, no. 2021, pp. 388–397, 2021.

[23] A. A. Shirzadi, H. Assadi, and E. R. Wallach, "Interface evolution and bond strength when diffusion bonding materials with stable oxide films," *Surface and Interface Analysis*, vol. 31, no. 7, pp. 609–618, 2001.

[24] M. S. Kenevisi and S. Mousavi Khoie, "A study on the effect of bonding time on the properties of Al7075 to Ti–6Al–4V diffusion bonded joint," *Materials Letters*, vol. 76, pp. 144–146, 2012.

[25] N. Kurgan, "Investigation of the effect of diffusion bonding parameters on microstructure and mechanical properties of 7075 aluminium alloy," *International Journal of Advanced Manufacturing Technology*, vol. 71, no. 9-12, pp. 2115–2124, 2014.

[26] Y. Wei, W. Aiping, Z. Guisheng, and R. Jialie, "Formation process of the bonding joint in Ti/Al diffusion bonding," *Materials Science and Engineering*, vol. 480, no. 1-2, pp. 456–463, 2008.

[27] T. Lin, C. Li, X. Si et al., "An investigation on diffusion bonding of Cu/Cu using various grain size of Ni interlayers at low temperature," *Materialia*, vol. 14, Article ID 100882, 2020.

[28] S. S. Seyyed Afghahi, M. Jafarian, M. Paidar, and M. Jafarian, "Diffusion bonding of Al 7075 and Mg AZ31 alloys: process parameters, microstructural analysis and mechanical properties," *Transactions of Nonferrous Metals Society of China*, vol. 26, no. 7, pp. 1843–1851, 2016.

[29] F. Wu, W. Chen, B. Zhao, H. Hou, W. Zhou, and Z. Li, "Diffusion bonding of 1420 Al–Li alloy assisted by pure aluminum foil as interlayer," *Materials*, vol. 13, no. 5, p. 1103, 2020.

[30] N. Özdemir, M. Aksoy, and N. Orhan, "Effect of graphite shape in vacuum-free diffusion bonding of nodular cast iron with gray cast iron," *Journal of Materials Processing Technology*, vol. 141, no. 2, pp. 228–233, 2003.

[31] J. Pilling and N. Ridley, "Solid state bonding of superplastic AA 7475," *Materials Science and Technology*, vol. 3, no. 5, pp. 353–359, 1987.

[32] Q. Jia, Z. Lai, H. Zhang et al., "Mechanism of ultrasonic-assisted transient liquid phase bonding of 6061 Al alloy with cladded Zn-Al alloy in air," *Journal of Materials Processing Technology*, vol. 286, Article ID 116823, 2020.

[33] Y. Liu, G. Wang, Y. Chen et al., "Air atmosphere diffusion bonding of Al–Mg–Li alloy using Cu nano-coating interlayer: microstructural characterization and formation mechanisms," *Materials and Design*, vol. 215, no. 2022, Article ID 110431, 2022.

[34] I. M. Barta, "Low temperature diffusion bonding of aluminum alloys," *Welding Journal*, vol. 43, pp. 241s–247s, 1964.

[35] A. S. T. M. Standard, *E407-07: Standard Practice for Microetching Metals and Alloys*, ASTM International, West Conshohocken, PA, USA, 2012.

[36] Astm E92-17, "Standard Test Methods for Vickers Hardness and Knoop Hardness of Metallic Materials," ASTM International, 2017, https://www.astm.org/e0092-17.html.

[37] J. Xiong, Y. Peng, M. Samiuddin, L. Yuan, and J. Li, "Common mechanical properties of diffusion bonded joints and their corresponding microstructure features," *Journal of Materials Engineering and Performance*, vol. 29, no. 5, pp. 3277–3286, 2020.

[38] S. Venugopal and G. Mahendran, "Effect of operation parameters on diffusion bonded AA5083, AA6082 and AA7075 aluminum alloys," *Transactions of the Indian Institute of Metals*, vol. 71, no. 9, pp. 2185–2198, 2018.

[39] C. S. Lee, H. Li, and R. S. Chandel, "Vacuum-free diffusion bonding of aluminium metal matrix composite," *Journal of Materials Processing Technology*, vol. 89-90, pp. 326–330, 1999.